Elucidation of the Reaction Mechanism of Catalytic Reaction Coupling of Ethylbenzene Dehydrogenation with Nitrobenzene Hydrogenation over MoO_3/TiO_2 Catalysts

Peng Yu, Zhengyang Yang, Zhiyong Gu and Hsi-Wu Wong*

Department of Chemical Engineering, University of Massachusetts Lowell

One University Ave., Lowell, MA 01854, USA

*Corresponding author, email: hsiwu_wong@uml.edu

Abstract

Catalytic coupling of ethylbenzene (EB) dehydrogenation with nitrobenzene (NB) hydrogenation offers potential economical and energetic benefits. However, several studies in the literature have shown that NB conversion could be higher than that of EB, violating the law of mass conversion. This work provides a new understanding of this reaction coupling scheme over MoO_3/TiO_2 catalysts to elucidate this scientific mystery. Our results showed that EB and NB have different adsorption rates on the TiO_2 surfaces, resulting in higher NB conversion. In addition, three distinct reaction schemes, each follows a different EB to NB stoichiometric ratio, were identified on the MoO_3 surfaces. The occurrence of the reactions is dependent on catalyst pretreatment by hydrogen reduction and the amount of oxygen vacancies on the surfaces. Our work explains why mass conservation was not satisfied in some previous studies due to the incorrect reaction stoichiometry used for analyzing the reactant conversions.

Keywords: Ethylbenzene dehydrogenation; Nitrobenzene hydrogenation; Reaction coupling; Molybdenum oxide; Titanium dioxide

1. Introduction

Styrene production from catalytic dehydrogenation of ethylbenzene (EB) (Reaction 1) is one of the most important reactions in the petrochemical industry [1-4]. Typically, iron oxides are the catalysts of choice with a reaction temperature between 400 and 550 °C. This reaction is highly endothermic (117 kJ/mol), and it is thermodynamic unfavorable with limited equilibrium conversion. As a result, a large amount of superheated steam is supplied to provide the needed heat and to shift the reaction equilibrium by lowering the concentrations of the species involved [5, 6].

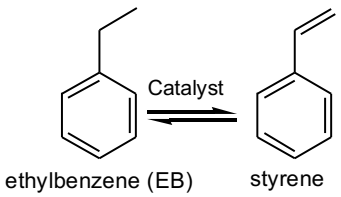

$$+ \quad H_2 \qquad \Delta H^0_{298k} = 117 \text{ kJ/mol} \qquad (1)$$

Several strategies have been studied to shift the equilibrium of EB dehydrogenation by removing one of its products, H_2. One strategy is to utilize a membrane reactor [7-10], allowing selective removal of H_2 from the catalyst bed. Another strategy is to couple EB dehydrogenation with a hydrogen depleting reaction, such as reverse water−gas shift reaction [5, 11-14], benzene hydrogenation [15], CO_2 methanation [16], and nitrobenzene hydrogenation [17-21]. Sun et al. [5, 11] studied the coupling of EB dehydrogenation with reverse water−gas shift reaction over iron and vanadium catalysts supported on activated carbon. The conversion of EB was greatly improved by the reaction coupling due to the simultaneous removal of the hydrogen in the product stream. High EB conversion (50−60%) and styrene selectivity (95−98%) were achieved at 550 °C. Abashar et al. [15] studied the coupling of EB dehydrogenation and benzene hydrogenation for simultaneous production of styrene and cyclohexane. The conversion of EB reached approximately 100% when reaction coupling was performed. Qin et al. [16] compared the benefits of coupling EB dehydrogenation with reverse water−gas shift, CO_2 methanation, and NB

hydrogenation. It was found that the equilibrium conversion of EB dehydrogenation was greatly enhanced by reaction coupling, especially with NB hydrogenation, where the equilibrium conversion reached 98.5% at 400 °C compared to 3.5% without reaction coupling.

It was apparent that coupling EB dehydrogenation with NB hydrogenation (Reaction 2) in one reaction stream offers significant benefits. In addition to removing the need for hydrogen in NB hydrogenation, the large energy released from NB hydrogenation (−464.3 kJ/mol) can be utilized for the endothermic EB hydrogenation [17-21]. Sun et al. [17] investigated EB dehydrogenation in the presence of NB over γ-Al_2O_3, ZSM-5, activated carbon, and supported platinum on activated carbon at 400 °C. They observed that the conversion of EB was greatly improved via reaction coupling over Pt (0.02 wt%)/AC catalyst. The highest EB conversion reached 33.8%, compared to 2.4% without the coupling, with a styrene selectivity reached 99.2%. Harikrishna et al. [18] studied the functionalities of Pd catalysts supported on spinel $MgAl_2O_4$ for the coupling of EB dehydrogenation with NB hydrogenation at atmospheric pressure between 400 and 550 °C, with Pd loading between 0.25 and 4 wt.%. It was concluded that a Pd loading of 0.5 wt% is optimal to achieve maximum conversions of EB and NB at 51.8% and 47.3% and selectivities to styrene and aniline at 91.4% and 100%, respectively. Itika et al. [19] studied MoO_2 catalyst on TiO_2−Al_2O_3 for this reaction coupling scheme at a temperature of 450 °C. The conversions for EB dehydrogenation and NB hydrogenation reached 28% and 61%, respectively, when the EB to NB molar ratio in the feed was 3 to 1. The selectivities to styrene and aniline reached almost 100%.

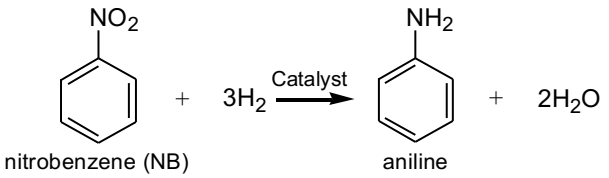

$$\Delta H^0_{298k} = -464.3 \text{ kJ/mol} \quad (2)$$

Although literature findings suggest that reaction coupling between EB dehydrogenation and NB hydrogenation provides potential promises, detailed understanding of its reaction mechanism is still limited, despite amble knowledge regarding individual mechanisms of EB dehydrogenation [22, 23] and NB hydrogenation [24, 25] in the literature. Following the hypothesized coupled reaction scheme, as shown in Reaction 3, three moles of hydrogen gas generated by EB dehydrogenation are needed per mole of NB hydrogenation. Consequently, if EB and NB are fed at a molar ratio of 3, the conversion of NB should always be lower than that of EB, which was observed in Harikrishna et al. [18]. However, several other studies [17, 19] showed that when EB and NB were fed at a molar ratio of 3, the conversion of NB could be more than 2 times higher than that of EB. This is clearly violating the law of mass conversion, suggesting that the stoichiometry of the coupled reaction does not always follow the hypothesized Reaction 3. The mechanistic-level understanding of the coupled reaction scheme is clearly needed to elucidate the conflicting findings regarding mass conservation in the literature.

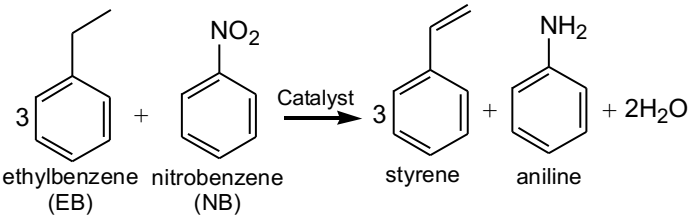

$$\Delta H^{0}_{298k} = -112.1\ \text{kJ/mol} \quad (3)$$

To provide a new understanding of reaction coupling between EB dehydrogenation and NB hydrogenation in this work, catalyst activity measurement experiments were performed using supported MoO_3/TiO_2 and unsupported MoO_3 catalysts at 350 °C with different EB to NB molar ratio in the feed. The effects of the TiO_2 support, catalyst pretreatment, and oxygen vacancies on MoO_3 surfaces on the reaction stoichiometry and surface reaction pathways were studied.

2. Methodology

2.1 Catalyst preparation and characterizations

MoO_3 supported on TiO_2 was prepared via wet impregnation, with a target MoO_3 loading of 10 wt%. Ammonium molybdate (para) tetrahydrate (99%, Alfa Aesar) was used as the precursor of MoO_3. For each catalyst sample, approximately 0.54 g of TiO_2 (titanium (IV) oxide, nanopowder, 21 nm primary particle size, ≥99.5% trace metals basis, Sigma-Aldrich) was used as the support and was directly weighted and dispersed in 50 ml deionized water via ultrasonication. 0.5 ml of ammonium molybdate (para) tetrahydrate solution was added into the aqueous suspension under magnetic stirring. The aqueous suspension was stirred continuously overnight and subsequently dried at 80 °C. The dried samples were then calcinated at 500 °C for 4 h in a furnace (Barnstead Thermolyne Corporation, Type 1400 Furnace). Bare MoO_3 (99.5%, Alfa Aesar) catalysts were also purchased and used in experiments for comparison.

Surface area measurements were conducted using a Quantachrome Autosorb 3b Automatic Surface Area and Pore Size Analyzer. The surface area of the bare support and the catalyst samples were measured from nitrogen adsorption−desorption at −195.79 °C (liquid nitrogen temperature) based on the Brunauer–Emmett–Teller (BET) theory [26]. Transmission electron microscopy (TEM, Philips CM12) was used to characterize the morphology of the nanoscale TiO_2 support and the synthesized catalysts. The samples for the TEM analysis were dispersed in ethanol via ultrasonication and then mounted on lacey-carbon-film-coated copper grids (Electron Microscopy Science, LC200−Cu) before imaging.

2.2 Catalyst activity measurements

Experiments of catalytic reaction coupling were carried out in a continuous quartz fixed−bed

reactor [27] at 350 °C at atmospheric pressure. This low temperature was chosen because experiments of EB dehydrogenation, NB hydrogenation, or the coupling of the two reported in the literature did not observe significant coke formation from the pyrolysis of the reactants (i.e., EB or NB) at this temperature [17-19, 21]. Catalyst of 200 mg was loaded in a bed of 1.5 inch in length, supported with quartz wool to contain the catalysts and to improve heat transfer for keeping the bed isothermal. The outer diameter of the quartz tube was 0.5 inch, and the inner diameter was 0.375 inch. A type-K thermocouple (OMEGA, KMQSS−062U−12) was positioned inside the catalyst bed to measure the reaction temperature. Prior to the reaction the catalyst was reduced under a H_2 (Airgas, 99.999%) flow rate of 30 ml/min for different duration (1−4 hrs) at 550 °C. The catalyst bed was then cooled to the reaction temperature (350 °C) before the delivery of the reactants. Different molar ratios of EB (Alfa Aesar, 99%) and NB (Acros Organics, 99%) were delivered by a syringe pump (KDS LEGATO 110, KD Scientific) into a heated line at a total feed rate between 4 and 8 μL/min. Nitrogen gas (Airgas, 99.998%), controlled by a flowmeter (Porter VCD–1000), was used as a carrier gas. Both the gas and liquid lines were heated to a temperature of 250 °C. The products were collected at regular intervals of 15 or 30 minutes in two ice−water traps and subsequently analyzed by gas chromatography (GC).

2.3 Products analysis

Identification of the reaction products was achieved using a Shimadzu GC2010 Plus GC equipped with a mass spectrometer (MS). 1 μL of sample was injected into the GC/MS system equipped with a Shimadzu SH-RXi-5Sil MS column (30 m), with a split ratio of 20. High purity helium (99.999%, Airgas) was used as a carrier gas in the column with a constant flow rate of 88.8 mL/min. The inlet temperature was set at 285 °C. The programmed temperature regime for the GC

oven was: start at 35 °C, hold for 7 minutes, ramp up to 185 °C at 7.5 °C/min, and ramp up to 285 °C at 20°C/min. The temperature of the MS detector was set at 285 °C.

Quantification of the reaction products was achieved using a Shimadzu GC2010 Plus GC with a flame ionization detector (FID). 1 μL of the sample was injected into the GC/FID system equipped with a Shimadzu Rxi-5ms column (15 m). The GC was programmed with the following inlet operating parameters: high purity helium carrier gas set at a constant flow pressure of 22.1 kPa, inlet temperature set at 285 °C, and a split injection mode with split ratio of 150. The detector temperature was set at 285 °C, with an air flow rate of 400 mL/min, a hydrogen gas flow rate of 40 mL/min, and a makeup gas flow rate of 30 ml/min. The GC oven was programmed with the following temperature regime: start at 35 °C, hold for 7 minutes, ramp up to 87.5 °C at 7.5 °C /min and hold for 2 minutes, ramp to 185 °C at 7.5 °C /min, and ramp to 285 °C at 20 °C /min.

The ethylbenzene conversion and the yield of each ethylbenzene−derived product were calculated on per mass basis as:

$$Conversion\ (\%) = \frac{\sum_i m_i}{\sum_i m_i + m_{ethylbenzene}} \times 100\ \%$$

$$Yield\ (\%) = \frac{m_i}{\sum_i m_i + m_{ethylbenzene}} \times 100\ \%$$

where m_i and $m_{ethylbenzene}$ are the mass flow rates of ethylbenzene−derived product i and unreacted ethylbenzene in the product stream, respectively. Similarly, the nitrobenzene conversion and the yield of each nitrobenzene−derived product were calculated as:

$$Conversion\ (\%) = \frac{\sum_j m_j}{\sum_j m_j + m_{nitrobenzene}} \times 100\ \%$$

$$Yield\ (\%)\ =\ \frac{m_j}{\sum_j m_j + m_{nitrobenzene}} \times 100\ \%$$

where m_j and $m_{nitrobenzene}$ are the mass flow rates of nitrobenzene−derived product j and unreacted nitrobenzene in the product stream, respectively. Finally, a collection ratio is defined in our work as:

$$Collection\ ratio = \frac{\sum_i n_i + n_{ethylbenzene}}{\sum_j n_j + n_{nitrobenzene}}$$

where n_i, n_j, $n_{ethylbenzene}$, and $n_{nitrobenzene}$ represent the molar flow rates of ethylbenzene−derived product i, nitrobenzene−derived product j, unreacted ethylbenzene, and unreacted nitrobenzene in the product stream, respectively. This ratio depicts the amount of EB and its derived products relative to NB and its derived products in the product stream.

3. Results and Discussion

The coupled EB dehydrogenation and NB hydrogenation reaction was first carried out over the synthesized MoO_3/TiO_2 catalyst at 350 °C. The EB and NB were fed at a molar ratio of 3. The conversions of EB and NB and the selectivities to styrene and aniline from these experiments are shown in Fig. 1. The selectivity to aniline reached almost 100% and the selectivity to aniline reached approximately 96% (with 4% selectivity to benzene as the major side product). The conversion of NB was initially higher than that of EB. Both trends were consistent with what were reported in the literature [17, 19]. Assuming that the coupled reaction follows the hypothesized Reaction 3, higher conversion of NB than that of EB is clearly violating the law of mass conservation, as stated earlier. Since this phenomenon was only observed during the first hour, it may be caused by several possible factors at early stages of the catalyst surfaces, including relative

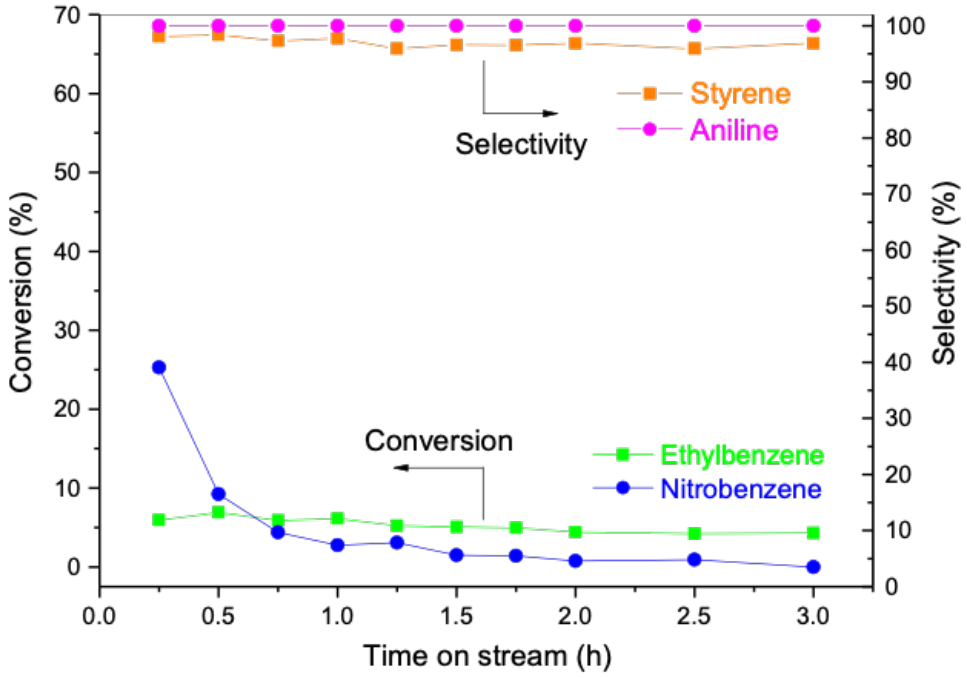

Fig. 1 The conversions of ethylbenzene (EB) and nitrobenzene (NB) and the selectivities to styrene and aniline resulted from the reaction coupling of EB dehydrogenation and NB hydrogenation over the MoO_3/TiO_2 catalyst at 350 °C. The EB and NB were fed at a molar ratio of 3.

adsorption rates of EB and NB, abundance of surface adsorbed hydrogen from pretreatment, and amount of surface oxygen vacancies. These hypothesized factors are examined individually in this work.

3.1 Effect of adsorption rates of EB and NB on catalyst surfaces

It is possible that the initial NB adsorption rate on the surfaces was faster that of EB, resulting in higher NB conversion. To test this hypothesis, the collection ratio as a function of time-on-stream was plotted in Fig. 2. This ratio depicts the relative amount of EB and EB−derived products to NB and NB−derived products in the product stream. Since EB and NB were fed at a molar ratio of 3, the collection ratio should remain at 3 if there was no difference in EB and NB adsorption rates on the catalyst surfaces. However, our results show that this ratio reached as high as 8 for the synthesized MoO_3/TiO_2 catalyst during the first half hour, suggesting that more EB and its derived

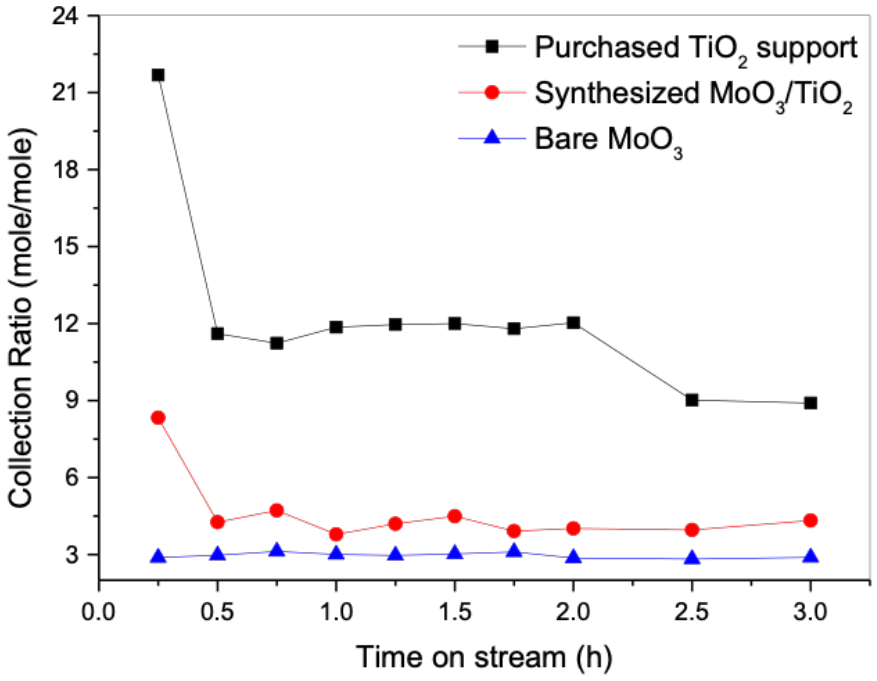

Fig. 2 The evolution of collection ratio as a function of time-on-stream for the purchased TiO_2 support, synthesized MoO_3/TiO_2, and bare MoO_3 without supports.

products were in the gas phase and more NB and its derived products were adsorbed on the catalyst surfaces during this period of time, supporting our hypothesis. This ratio decreased to approximately 4 with increased time-on-stream. The TEM images and EDAX spectra for the purchased TiO_2 support (Fig. 3A and C) and the synthesized MoO_3/TiO_2 catalyst (Fig. 3B and D) show that MoO_3 was covered uniformly on the TiO_2 surface for the synthesized catalyst, where Mo was observed in the EDAX spectra. The BET analysis suggested that the surface area of the synthesized MoO_3/TiO_2 catalyst was smaller at 39 m^2/g, compared to the bare TiO_2 support at 53 m^2/g, due to the larger particle size caused by the presence of the MoO_3 layers on TiO_2.

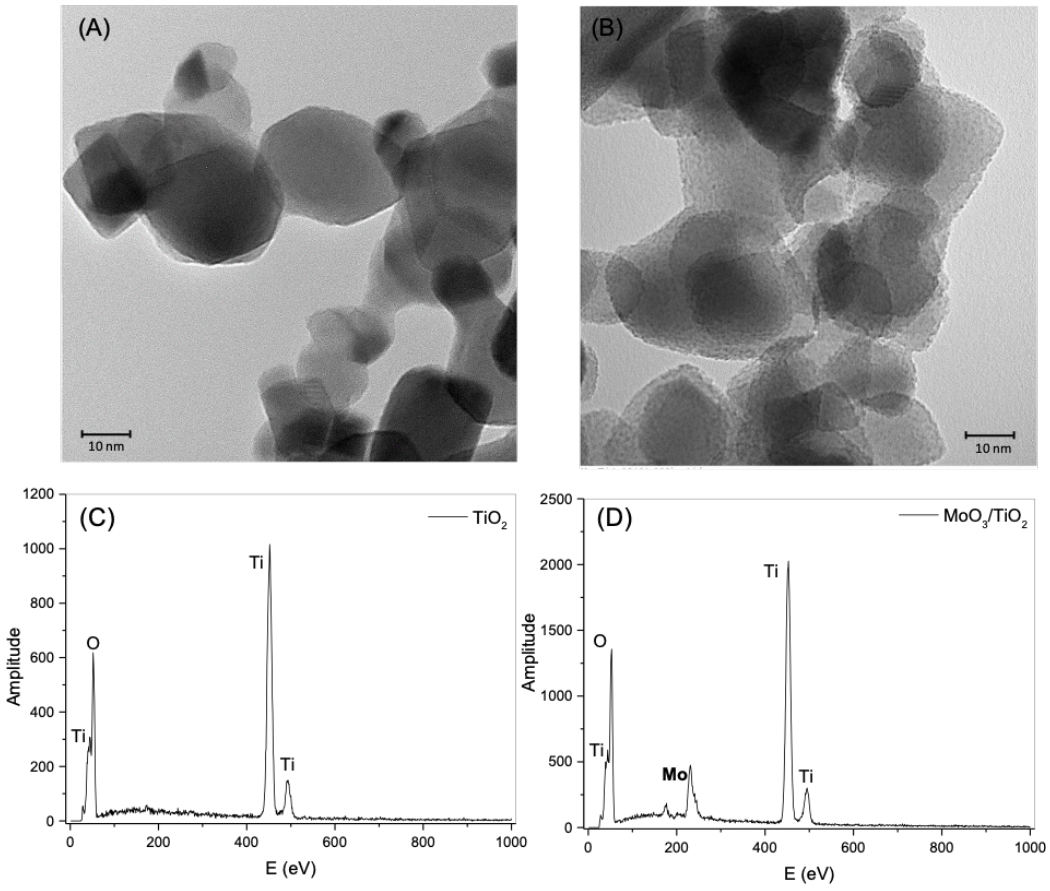

Fig. 3 TEM images and EDAX spectra of the purchased TiO_2 support (A and C) and the synthesized MoO_3/TiO_2 catalyst (B and D).

To further examine the difference in adsorption rates between TiO_2 and MoO_3, the experiments using only TiO_2 support (without MoO_3) was also performed. In these experiments, the amount of TiO_2 support was adjusted to have the same total surface areas as the synthesized MoO_3/TiO_2 catalyst. Our experiments showed that the collection ratio was even higher when the purchased TiO_2 support was used (black squares in Fig. 2), starting at approximately 22 before dropping to approximately 12. This suggests that NB or its derived products adsorb on the TiO_2 support much more easily than EB and its derived products. The difference in EB and NB adsorption rates subsequently contributed to the higher NB conversion.

Note that although the total surface areas of the TiO_2 support (53 m^2/g) and synthesized MoO_3/TiO_2 (39 m^2/g) were approximately the same, significant fraction of the synthesized MoO_3/TiO_2 surface was covered by MoO_3 (see the TEM image Fig. 3B) that did not show preference to NB and EB adsorption. This suggests that the actual surface that had preference to NB over EB is much higher on the pure TiO_2 support than that on MoO_3/TiO_2, resulting in the collection ratio not leveled off within the 3-hour time-on-stream period for pure TiO_2.

While the difference of adsorption rates between EB and NB on TiO_2 contributed to the difference of their conversions, this does not eliminate the possible effects caused by MoO_3. To investigate the roles of MoO_3, experiments with the purchased MoO_3 catalyst without the TiO_2 support were further conducted. In this case, the collection ratio was found to be around 3 (blue triangles in Fig. 2), meaning that EB and NB have almost the same adsorption rates on the MoO_3 surface, again confirming that TiO_2 support results in different adsorption rates of EB and NB on catalyst surfaces.

3.2 Effect of surface adsorbed hydrogen caused by reduction

The majority of the catalysts used in the literature for the coupling between EB dehydrogenation and NB hydrogenation were reduced under H_2 atmosphere prior to reactions [17-19]. The H_2 used in the reduction process could produce surface adsorbed hydrogen atoms that promote NB hydrogenation, causing higher NB conversion than expected. To examine this possible effect, the bare MoO_3 catalyst was reduced by H_2 for 0 hour, 2 hours, and 4 hours, respectively, before they were used in the experiments. In this set of experiments, MoO_3 was reduced by H_2 at 550 °C in the quartz reactor. After the reduction, the reactor tube was removed from the furnace and kept at room temperature for more than 12 hours before being inserted back into the furnace at 350 °C. Fig. 4 shows that longer H_2 reduction time indeed resulted in higher aniline yields, suggesting that hydrogen atoms adsorbed on the catalyst surfaces, produced during the catalyst pretreatment process, played a key role in the elevated, non-stoichiometric aniline yields.

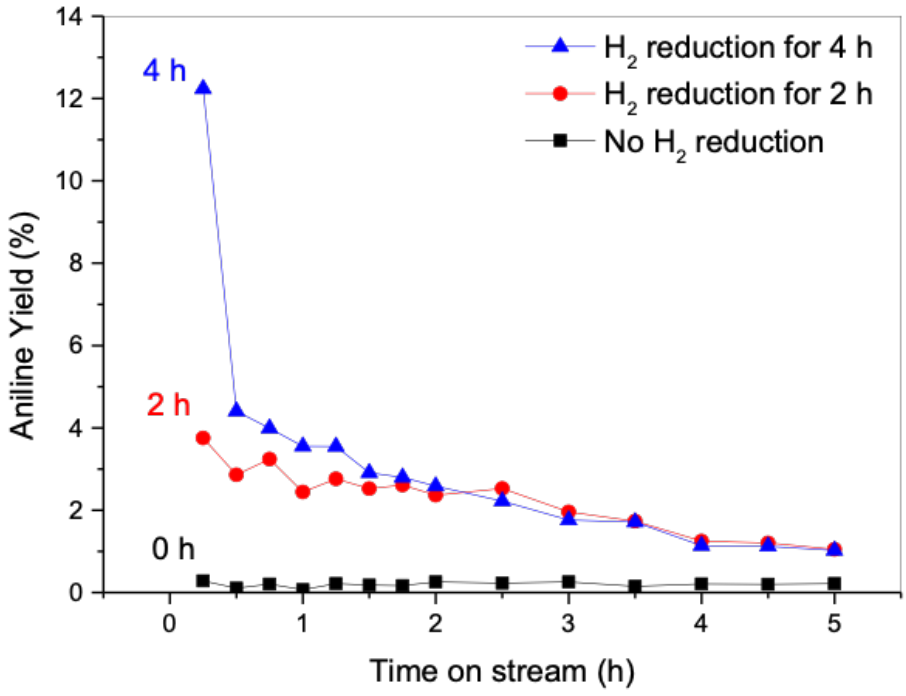

Fig. 4 The yields of aniline with catalysts reduced by different durations of H_2 for the coupling of EB dehydrogenation with NB hydrogenation.

One of the key assumptions made in our work was minimal coking at this low reaction temperature of 350 °C. To confirm this assumption, the spent catalyst used for the 2-hour reduction experiment after the entire time-on-stream procedure was further burnt off with air at a flow rate of 23 ml/min at 550 °C. The exhaust gas was collected in a Tedlar® bag and analyzed by GC/TCD. It was found that the amount of carbon atoms associated with the exhaust CO_2, possibly resulted from the combustion of coke on the spent catalyst, could only account for at most 0.1% of initial NB in the feed (assuming all coke was produced from NB rather than EB). Since NB conversion in this particular experiment reached as high as 4%, this clearly shows that coking reaction is not dominant at this low (350 °C) reaction temperature and is not a major reaction pathway to provide hydrogen for NB conversion into aniline.

To further understand the role of surface adsorbed hydrogen atoms, reduced catalysts were also used for the NB hydrogenation reaction without the coupling EB dehydrogenation. Pure NB with a flow rate of 2 μL/min was delivered by the syringe pump, with nitrogen used as a carrier gas. Two control experiments were also performed for comparison using: (1) MoO_3 catalyst without H_2 reduction and (2) H_2 reduced MoO_3 catalyst followed by N_2 treatment (at 30 ml/min) for 1 hour, respectively. Fig. 5 shows that no aniline was observed in both control experiments. On the contrary, the aniline yield reached as high as 5% when the catalyst was reduced by H_2 without any other H_2 sources (e.g., without the delivery of EB). This suggests that the hydrogen atoms adsorbed on the MoO_3 surfaces facilitate aniline formation from NB, likely following the scheme (Reaction 4).

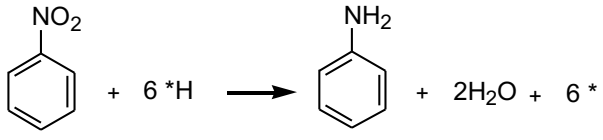

(4)

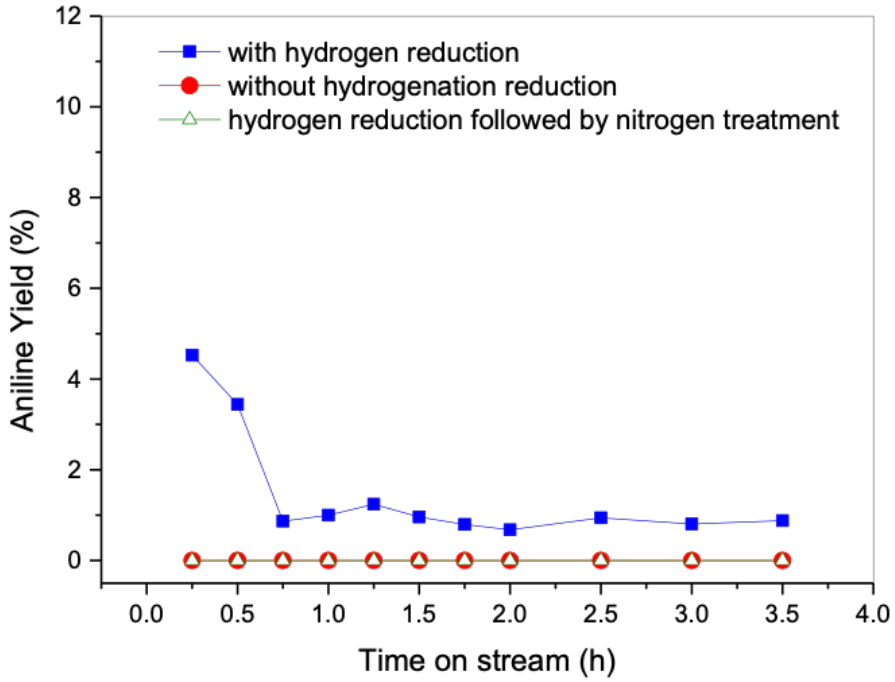

Fig. 5 The aniline yields from neat NB hydrogenation without the coupling of EB dehydrogenation over catalysts with or without H_2 pretreatment.

3.3 Effect of surface oxygen vacancies and three zones of reactions

Reducible metal oxide catalysts have been extensively studied for various chemical synthesis reactions [28-35]. Most reactions on reducible metal oxides follow Mars−van Krevelen mechanism [36]. MoO_3, as one of the reducible metal oxides, has been utilized by many applications such as acrolein synthesis [37], hydrocracking [38, 39], and recently bio−oil hydrodeoxygenation [40]. Specifically, Román-Leshkov et al. [41-44] investigated hydrodeoxygenation of biomass-derived oxygenates into unsaturated hydrocarbons over MoO_3 catalysts. It is suggested that MoO_3 reduction by H_2 creates oxygen vacancies on the catalyst surfaces. These oxygen vacancies can then act as oxygen removal sites to attract oxygen atoms of an oxygenated species, promoting C–O bond cleavage. Before reaction coupling between EB dehydrogenation and NB hydrogenation, oxygen vacancies should be similarly created on the MoO_3 surfaces after H_2 reduction. The created oxygen vacancies could play a similar role of

removing the oxygen atoms of NB. The deoxygenated NB could subsequently react with surface adsorbed hydrogen atoms to produce aniline. The overall reaction follows Reaction 5. In this case, when oxygen vacancies (denoted as *) are available, only one mole of EB is needed to react with one mole of NB to produce one mole of aniline. Note that the experiment using only NB in the feed without EB, over catalyst reduced by H_2 and subsequently treated with N_2 to create a surface with only oxygen vacancies and no hydrogen, did not give significant aniline yields (i.e., green open triangles in Fig. 5). This suggests that oxygen vacancies on the surface alone could not convert NB into aniline without the presence of a hydrogen source (such as EB in Reaction 5).

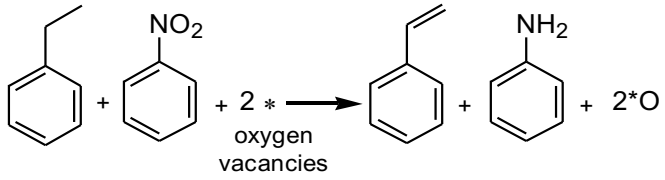

(5)

Once the adsorbed hydrogen atoms and oxygen vacancies have been depleted on the MoO_3 surface, the coupled reaction should proceed with the conventional hypothesized Reaction 3, where three moles of EB react with one mole of NB to produce one mole of aniline. Consequently, three distinct reaction schemes (Reactions 3-5) are possible to take place during the coupling of EB dehydrogenation with NB hydrogenation, as illustrated in Fig. 6. Each of the three reactions follows a distinct EB to NB stoichiometric ratio. Note that this does not prevent EB dehydrogenation from occurring independently, although EB dehydrogenation would not contribute to the nonstoichiometric higher NB conversion than EB conversion.

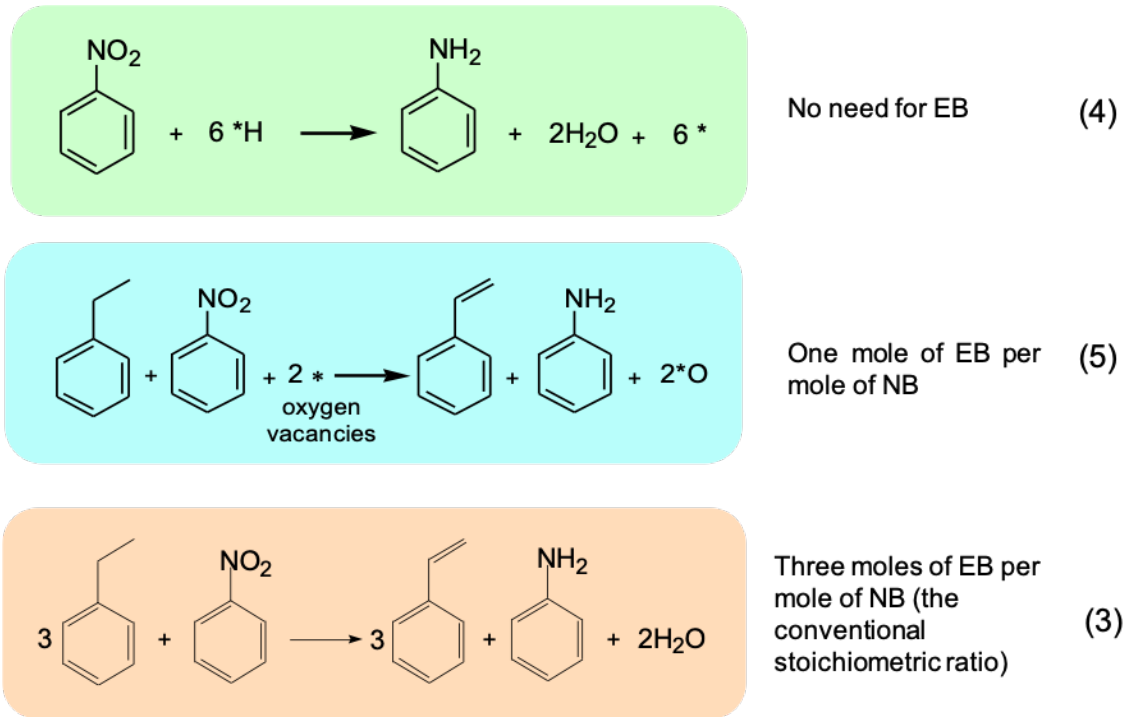

Fig. 6 Three possible reactions on the MoO_3 surfaces during the coupling of EB dehydrogenation with NB hydrogenation. Each reaction represents a unique EB to NB stoichiometric ratio.

To determine the relative importance of the three hypothesized reaction schemes during the coupling of EB dehydrogenation with NB hydrogenation over reduced MoO_3, EB and NB were fed at three different molar ratios, with three different catalyst reduction times (no H_2 reduction, 2 h and 4 h H_2 reduction, respectively). Our experiments showed that the collection ratios in these experiments were close to EB to NB molar ratios in the feed (Fig. 7 B, D, and F), suggesting that there was no discrepancy between EB and NB adsorption on the MoO_3 surfaces, unlike what was observed for the MoO_3/TiO_2 catalysts. This further confirmed that the difference in EB and NB adsorption was solely caused by the TiO_2 support. For experiments using catalysts pretreated by H_2, the initial ratios of aniline to styrene yields were all higher than the corresponding EB to NB molar ratios in the feed (green region), suggesting that there existed abundant hydrogen atoms adsorbed on the MoO_3 surfaces produced from the pretreatment process. These surface adsorbed

hydrogen atoms reacted with NB to produce aniline (following Reaction 4). The ratios of aniline to styrene yields subsequently decreased to a level below the corresponding EB to NB molar ratios in the feed (blue region), suggesting a 1:1 stoichiometric coupling between EB and NB (following Reaction 5). The ratios of aniline to styrene yields eventually dropped to below one third of the EB to NB molar ratio in the feed (orange region), suggesting that both surface adsorbed hydrogen atoms and oxygen vacancies were depleted and the overall reaction followed the scheme presented by the conventional believed stoichiometric ratio illustrated in Reaction 3.

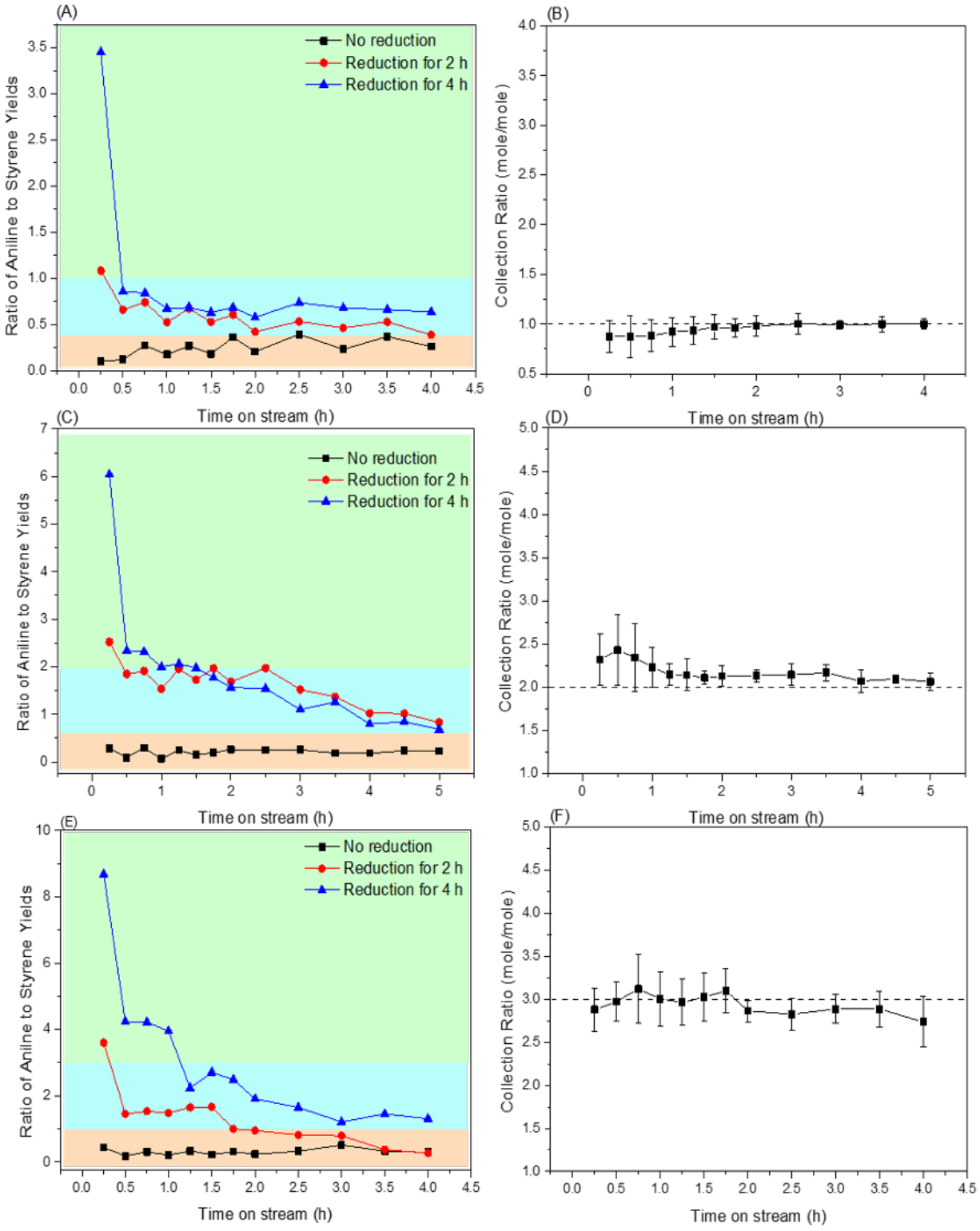

Fig. 7 The ratios of aniline to styrene yields and the corresponding collection ratios when EB and NB molar ratio in the feed were: (A) and (B) 1:1; (C) and (D) 2:1; (E) and (F) 3:1 (the corresponding collection ratios of the products suggest no adsorption effects).

4. Conclusion

Reaction coupling between ethylbenzene (EB) dehydrogenation and nitrobenzene (NB) hydrogenation was studied over supported MoO_3/TiO_2 and unsupported MoO_3 catalysts. The use of TiO_2 support results in faster NB adsorption on the surfaces. Our experimental results also suggest that reaction stoichiometry is dependent on the states of the MoO_3 catalysts. Three possible reaction schemes involving MoO_3 were proposed. The first reaction scheme was facilitated by surface adsorbed hydrogen atoms, where no EB was needed for NB hydrogenation to produce aniline. The second reaction scheme was driven by surface oxygen vacancies, where the stoichiometric ratio between EB and NB was 1:1. The third reaction scheme follows the conventional reaction coupling stoichiometry where three EB molecules are needed per NB molecule. Our work explains why mass conservation was not satisfied in some studies in the literature, where incorrect reaction stoichiometry was mistakenly used for analyzing conversions of EB and NB.

Acknowledgements

Funding supports from the National Science Foundation (CBET-1842101), UMass Lowell Research and Innovation Seed Grant, and UMass Lowell Faculty Startup Funds are greatly appreciated.

References

[1] W. Weiss, D. Zscherpel, R. Schlögl, Catalysis Letters, 52 (1998) 215-220.

[2] R. Schlögl, Angewandte Chemie International Edition, 54 (2015) 3465-3520.

[3] A. Miyakoshi, A. Ueno, M. Ichikawa, Applied Catalysis A: General, 219 (2001) 249-258.

[4] H. Knözinger, J. Weitkamp, Handbook of Heterogeneous Catalysis: Volume 3, Wiley-VCH, 1997.

[5] A. Sun, Z. Qin, J. Wang, Applied Catalysis A: General, 234 (2002) 179-189.

[6] J. Matsui, T. Sodesawa, F. Nozaki, Applied Catalysis, 67 (1990) 179-188.

[7] Y.L. Becker, A.G. Dixon, W.R. Moser, Y.H. Ma, Journal of Membrane Science, 77 (1993) 233-244.

[8] P. Quicker, V. Höllein, R. Dittmeyer, Catalysis Today, 56 (2000) 21-34.

[9] C. Hermann, P. Quicker, R. Dittmeyer, Journal of Membrane Science, 136 (1997) 161-172.

[10] J.C. Wu, P.K. Liu, Industrial & Engineering Chemistry Research, 31 (1992) 322-327.

[11] A. Sun, Z. Qin, S. Chen, J. Wang, Journal of Molecular Catalysis A: Chemical, 210 (2004) 189-195.

[12] S. Sato, M. Ohhara, T. Sodesawa, F. Nozaki, Applied Catalysis, 37 (1988) 207-215.

[13] N. Mimura, M. Saito, Catalysis Today, 55 (2000) 173-178.

[14] Y. Ohishi, T. Kawabata, T. Shishido, K. Takaki, Q. Zhang, Y. Wang, K. Takehira, Journal of Molecular Catalysis A: Chemical, 230 (2005) 49-58.

[15] M. Abashar, Chemical Engineering Processing: Process Intensification, 43 (2004) 1195-1202.

[16] Z. Qin, J. Liu, A. Sun, J. Wang, Industrial & Engineering Chemistry Research, 42 (2003) 1329-1333.

[17] A. Sun, Z. Qin, J. Wang, Catalysis Letters, 79 (2002) 33-37.

[18] Y. Harikrishna, V.P. Kumar, K. Ramu, K.V. Chary, V.V. Rao, Applied Petrochemical Research, 5 (2015) 71-80.

[19] K. Itika, G.V.R. Babu, T.B. Jayesh, K.S.R. Rao, B.M. Nagaraja, Catalysis Communications, 90 (2017) 27-30.

[20] A. Malaika, J. Gertig, P. Rechnia, A. Miklaszewska, M. Kozłowski, Arabian Journal of Chemistry, 12 (2019) 4947-4956.

[21] A. Malaika, P. Rechnia, B. Krzyżyńska, A. Tolińska, A. Kawałko, M. Kozłowski, Applied Catalysis A: General, 452 (2013) 39-47.

[22] Y. Sakurai, T. Suzaki, K. Nakagawa, N.-o. Ikenaga, H. Aota, T. Suzuki, Journal of Catalysis, 209 (2002) 16-24.

[23] B.B. Tope, R.J. Balasamy, A. Khurshid, L.A. Atanda, H. Yahiro, T. Shishido, K. Takehira, S.S. Al-Khattaf, Applied Catalysis A: General, 407 (2011) 118-126.

[24] L. Zhang, J. Jiang, W. Shi, S. Xia, Z. Ni, X. Xiao, RSC Advances, 5 (2015) 34319-34326.

[25] T. Sheng, Y.-J. Qi, X. Lin, P. Hu, S.-G. Sun, W.-F. Lin, Chemical Engineering Journal, 293 (2016) 337-344.

[26] S. Brunauer, P.H. Emmett, E. Teller, Journal of the American Chemical Society, 60 (1938) 309-319.

[27] P. Yu, H.-W. Wong, Chemical Engineering Science, 210 (2019) 115243.

[28] A.P.V. Soares, M.F. Portela, A. Kiennemann, Catalysis Reviews, 47 (2005) 125-174.

[29] J.M. Vohs, Chemical Reviews, 113 (2012) 4136-4163.

[30] M.A. Barteau, Chemical Reviews, 96 (1996) 1413-1430.

[31] A.B. Getsoian, V. Shapovalov, A.T. Bell, The Journal of Physical Chemistry C, 117 (2013)

7123-7137.

[32] A.B. Getsoian, A.T. Bell, The Journal of Physical Chemistry C, 117 (2013) 25562-25578.

[33] Z. Zhai, A.T. Bell, Journal of Catalysis, 308 (2013) 25-36.

[34] A. Ruiz Puigdollers, P. Schlexer, S. Tosoni, G. Pacchioni, ACS Catalysis, 7 (2017) 6493-6513.

[35] S.M. Schimming, G.S. Foo, O.D. LaMont, A.K. Rogers, M.M. Yung, A.D. D'Amico, C. Sievers, Journal of Catalysis, 329 (2015) 335-347.

[36] P. Mars, D.W. Van Krevelen, Chemical Engineering Science, 3 (1954) 41-59.

[37] G.W. Keulks, M.P. Rosynek, C. Daniel, Industrial & Engineering Chemistry Product Research, 10 (1971) 138-142.

[38] H. Al-Kandari, S. Al-Kandari, F. Al-Kharafi, A. Katrib, Energy Fuels, 23 (2009) 5737-5742.

[39] H. Al-Kandari, F. Al-Kharafi, A. Katrib, Catalysis Communications, 9 (2008) 847-852.

[40] D. Mei, A.M. Karim, Y. Wang, The Journal of Physical Chemistry C, 115 (2011) 8155-8164.

[41] T. Prasomsri, T. Nimmanwudipong, Y. Roman-Leshkov, Energy & Environmental Science, 6 (2013) 1732-1738.

[42] T. Prasomsri, M. Shetty, K. Murugappan, Y. Román-Leshkov, Energy & Environmental Science, 7 (2014) 2660-2669.

[43] M. Shetty, K. Murugappan, T. Prasomsri, W.H. Green, Y. Román-Leshkov, Journal of Catalysis, 331 (2015) 86-97.

[44] M. Shetty, B. Buesser, Y. Román-Leshkov, W.H. Green, The Journal of Physical Chemistry C, 121 (2017) 17848-17855.